

Mitigation of envelope instability through fast acceleration

Ji Qiang*

Lawrence Berkeley National Laboratory, Berkeley, CA 94720, USA

The space-charge driven envelope instability can be of great danger in high intensity accelerators. Linear accelerators were designed to avoid this instability by keeping the zero current phase advance per lattice period below 90 degrees. In this paper, we studied the acceleration effects on the instability in a periodic solenoid and radio-frequency (RF) focusing channel and a periodic quadrupole and RF focusing channel using a three-dimensional envelope model and self-consistent macroparticle simulations. Our results show that the envelope instability can be dramatically mitigated with a reasonable accelerating gradient in both channels. This suggests that the zero current phase advance might be above 90 degrees in linear accelerators where the accelerating gradient is sufficiently high and opens additional degrees of freedom of transverse and longitudinal focusing parameters in the accelerator design.

I. INTRODUCTION

In a periodic accelerator system, when the zero current phase advance through one lattice period is above 90 degrees, the envelope oscillation of a charged particle beam with finite current can become unstable [1, 2]. Such an envelope instability driven by the space-charge effects causes beam size blow up and potential particle losses inside the accelerator. In order to avoid the envelope instability, linear accelerators were designed with zero current phase advance per lattice period below 90 degrees [3–9]. However, the linear accelerator is not a perfect periodic system. In addition to the machine imperfections such as field amplitude error and misalignment error, the use of RF cavity acceleration breaks the longitudinal periodicity of the accelerator. The presence of RF acceleration helps damp the envelope oscillation and also modifies the transverse and longitudinal focusing strengths and space-charge forces. Previous studies have shown that resonances in a circular accelerator can be crossed without significantly affecting the beam quality if the crossing speed is sufficiently fast [10–13]. With the use of superconducting RF cavity in the linear accelerator, the high accelerating gradient from the cavity may help overcome the envelope instability. In this paper, we report on mitigating strong envelope instability of a proton beam through a solenoid-RF lattice and through a quadrupole-RF lattice with 120 degree zero current transverse and longitudinal phase advances.

The envelope instability in a periodic transport channel has been extensively studied theoretically and experimentally since the 1980s [1, 2, 14–31]. (Some of those studies were summarized in a recently published monograph [32].) It is the lowest order (second-order) collective mode instability driven by the direct space-charge effects and could present great danger in high intensity accelerator operation. Recently, an analysis of bunched beam stabilities in a periodic solenoid-RF and in a periodic quadrupole-RF transport channel was done using a three-dimensional (3D) envelope model without acceleration [33]. A number of instability stopbands were identified in that study when the zero current phase advance per lattice period is beyond 90 degrees. In this paper, we study the effects of acceleration on the instability of envelope oscillation in these two types of focusing channels.

II. THREE-DIMENSIONAL ENVELOPE INSTABILITY MODEL WITH ACCELERATION

In a linear accelerator, for a 3D uniform density ellipsoidal beam, the 3D envelope equations including acceleration are given as [34, 35]:

$$\frac{d^2 X}{ds^2} + \left(\frac{p'_0}{p_0}\right) \frac{dX}{ds} + k_x^2(s)X - \frac{Ku_0\pi\lambda_3}{l^2} G_{311}(X, Y, u_0T)X - \left(\frac{\delta}{lp_0}\right)^2 \frac{\epsilon_x^2}{X^3} = 0 \quad (1)$$

$$\frac{d^2 Y}{ds^2} + \left(\frac{p'_0}{p_0}\right) \frac{dY}{ds} + k_y^2(s)Y - \frac{Ku_0\pi\lambda_3}{l^2} G_{131}(X, Y, u_0T)Y - \left(\frac{\delta}{lp_0}\right)^2 \frac{\epsilon_y^2}{Y^3} = 0 \quad (2)$$

$$\frac{d^2 T}{ds^2} + 3\left(\frac{p'_0}{p_0}\right) \frac{dT}{ds} + k_t^2(s)T - \frac{Ku_0\pi\lambda_3}{l^2} G_{113}(X, Y, u_0T)T - \left(\frac{\delta}{lp_0u_0^2}\right)^2 \frac{\epsilon_t^2}{T^3} = 0 \quad (3)$$

*Electronic address: jqiang@lbl.gov

with

$$G_{lmn}(x, y, z) = \frac{3}{2} \int_0^\infty \frac{ds}{(x^2 + s)^{l/2}(y^2 + s)^{m/2}(z^2 + s)^{n/2}} \quad (4)$$

where X and Y are horizontal and vertical rms beam sizes normalized by the scaling length $l = c/\omega$, T is the rms longitudinal phase ($T = \omega\Delta t$), Δt denotes the rms time of flight difference between the individual particle and the reference particle, c is the speed of light in vacuum, ω is the RF angular frequency, $p_0 = mc\gamma_0\beta_0$ is the reference particle momentum, the prime denotes derivative with respect to distance s , k_x^2 , k_y^2 , k_t^2 represent the external focusing forces ($k_x(s) = k_y(s) = qB(s)/(2p_0)$ for solenoids and $k_{x,y}^2(s) = \pm qG(s)/p_0$ for quadrupoles, where B is the solenoid root mean-squared magnetic field along the axis and G is the quadrupole gradient, $k_t^2 = \omega q E_0 T_{tr} \sin(-\phi_s)/(mc^3\beta^3\gamma^3)$ for longitudinal RF focusing [36]), $u_0 = \gamma_0\beta_0$, $\delta = mc$, ϵ_x , ϵ_y , and ϵ_t are normalized rms emittances, and K is the generalized perveance associated with the space-charge strength given by:

$$K = \frac{qI}{2\pi\epsilon_0 p_0 v_0^2 \gamma_0^2} \quad (5)$$

where I is the average current of the beam, q is the charge of the particle, ϵ_0 is the vacuum permittivity, v_0 is the speed of the reference particle, and γ_0 is the relativistic factor of the reference particle. The quantity λ_3 is a constant depending on the distribution of the beam. It was pointed out in reference [34] that the space-charge form factor $\lambda_3 = 1/5\sqrt{5}$ for a uniform distribution depends only weakly on the type of distributions and is $1.01/5\sqrt{5}$ for a parabolic distribution and $1.05/5\sqrt{5}$ for a Gaussian distribution.

The above envelope equations can be linearized with respect to matched solutions as:

$$X(s) = X_0(s) + x(s) \quad (6)$$

$$Y(s) = Y_0(s) + y(s) \quad (7)$$

$$T(s) = T_0(s) + t(s) \quad (8)$$

where X_0 , Y_0 and Z_0 denote the matched envelope solutions and x , y and t denote small perturbations

$$x(s) \ll X_0(s), \quad y(s) \ll Y_0(s), \quad t(s) \ll T_0(s) \quad (9)$$

Let $\xi = (x, p_x, y, p_y, t, p_t)^T$, the equations of motion for the perturbations are given by:

$$\frac{d\xi}{ds} = A_6(s)\xi(s) \quad (10)$$

with the matrix A_6 given by:

$$A_6(s) = \begin{pmatrix} 0 & \frac{\delta}{lp_0(s)} & 0 & 0 & 0 & 0 \\ a_{21}(s) & 0 & a_{23}(s) & 0 & a_{25}(s) & 0 \\ 0 & 0 & 0 & \frac{\delta}{lp_0(s)} & 0 & 0 \\ a_{23}(s) & 0 & a_{43}(s) & 0 & a_{45}(s) & 0 \\ 0 & 0 & 0 & 0 & 0 & \frac{\delta}{lp_0(s)u_0^2(s)} \\ a_{25}(s) & 0 & a_{45}(s) & 0 & a_{65}(s) & 0 \end{pmatrix} \quad (11)$$

where

$$a_{21}(s) = -\frac{lp_0}{\delta} k_x^2 - 3\frac{\delta}{lp_0} \frac{\epsilon_x^2}{X_0^4} - \frac{Ku_0^2\pi\lambda_3}{l} (3X_0^2 G_{511} - G_{311}) \quad (12)$$

$$a_{23}(s) = -\frac{Ku_0^2\pi\lambda_3}{l} X_0 Y_0 G_{331} \quad (13)$$

$$a_{25}(s) = -\frac{Ku_0^4\pi\lambda_3}{l} X_0 T_0 G_{313} \quad (14)$$

$$a_{43}(s) = -\frac{lp_0}{\delta} k_y^2 - 3\frac{\delta}{lp_0} \frac{\epsilon_y^2}{Y_0^4} - \frac{Ku_0^2\pi\lambda_3}{l} (3Y_0^2 G_{151} - G_{131}) \quad (15)$$

$$a_{45}(s) = -\frac{Ku_0^4\pi\lambda_3}{l} Y_0 T_0 G_{133} \quad (16)$$

$$a_{65}(s) = -\frac{lp_0 u_0^2}{\delta} k_z^2 - 3\frac{\delta}{lp_0 u_0^2} \frac{\epsilon_t}{T_0^4} - \frac{Ku_0^4\pi\lambda_3}{l} (3u_0^2 T_0^2 G_{115} - G_{113}) \quad (17)$$

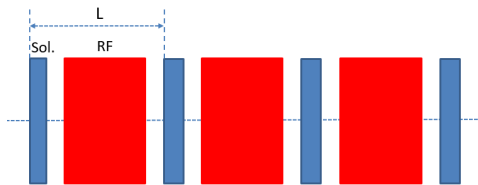


FIG. 1: Schematic plot of a periodic solenoid and RF channel.

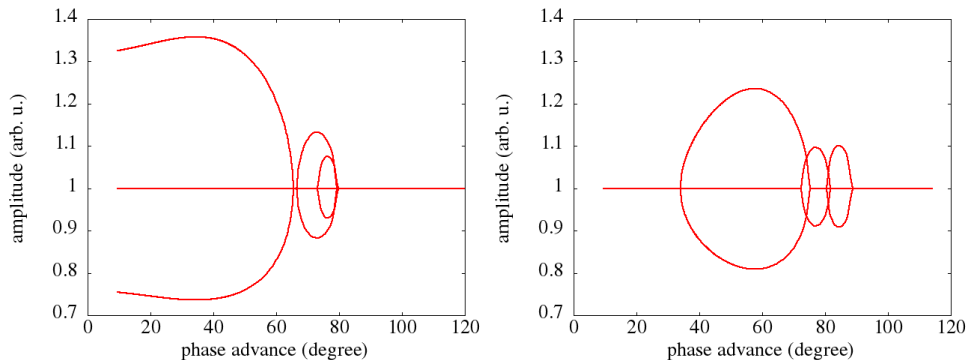


FIG. 2: The 3D envelope mode growth rate amplitudes as a function of depressed transverse phase advance with 120 degree zero current transverse and longitudinal phase advances in the periodic solenoid-RF channel without acceleration (left) and with 8 MV/m accelerating gradient (right).

Let solution $\xi(s) = M_6(s)\xi(0)$, substituting this equation into Eq. 10 results in

$$\frac{dM_6(s)}{ds} = A_6(s)M_6(s) \quad (18)$$

where $M_6(s)$ denotes the 6×6 transfer matrix solution of $\xi(s)$ and $M_6(0)$ is a 6×6 unit matrix. The above ordinary differential equation can be solved using the matched envelope solutions and numerical integration. The stability of these envelope perturbations is determined by the eigenvalues of the transfer matrix $M_6(L)$ through one lattice period. For the envelope oscillation to be stable, all six eigenvalues (three pairs) of the $M_6(L)$ have to stay on the unit circle. The amplitude of the eigenvalue gives the envelope mode growth (or damping) rate through one lattice period, while the phase of the eigenvalue yields the mode oscillation frequency. When the amplitude of any eigenvalue is greater than one, the envelope oscillation becomes unstable.

III. MITIGATION OF THE ENVELOPE INSTABILITY IN A SOLENOID AND RF CHANNEL

We first studied the mitigation of the envelope instability in a transverse solenoid focusing and longitudinal RF accelerating and focusing channel. A schematic plot of this channel is shown in Fig. 1. Each period of the accelerator lattice consists of a 0.1 meter solenoid, a 0.1 meter drift, a 0.4 meter RF cavity, and 0.1 meter drift. The proton bunch has a kinetic energy of 10 MeV and normalized rms emittances of 0.2 μm in all three directions. Figure 2 shows the envelope mode growth rate amplitudes as a function of depressed transverse phase advance inside the above lattice with 120 degree zero current transverse and 120 degree zero current longitudinal phase advances without and with 8 MV/m accelerating gradient inside the RF cavities. Here, the smaller depressed phase advance corresponds to the stronger space-charge defocusing effects and the higher proton beam bunch intensity. Without acceleration, the beam shows strong envelope instability. There are three instability stopbands below about 80 degree depressed transverse phase advances. The stopband below 65 degree depressed tune is due to the confluent resonance between two envelope oscillation modes. The other two stopbands are due to the half-integer parametric resonance between the focusing lattice and the envelope oscillation modes. With the presence of acceleration, the above envelope instability stopbands are significantly modified. The width of stopband is reduced from about 80 degrees to about 50 degrees. The instability growth rate maximum amplitude is also reduced from nearly 1.4 to about 1.2.

In order to study the effects of acceleration on the envelope instability, we also carried out self-consistent macroparticle simulations using a 3D particle-in-cell code, IMPACT [37, 38]. We first selected an unstable point inside the

depressed phase advance stopband with large instability growth rate. The transverse depressed phase advance for this point is 40 degrees, which represents a strong space-charge tune depression ratio of 0.33. We assumed 10% mismatch in all three directions of an initial Waterbag distribution and used about 625,000 macroparticles and $64 \times 64 \times 64$ grid points in the simulations. Figure 3 shows the horizontal and longitudinal rms size (normalized by the matched rms size) evolution and the emittance growth evolution through the above lattice without and with 8 MV/m accelerating gradient in the RF cavities. Here, we assumed that proton beam energy increases linearly inside the RF cavities due to the RF acceleration. Without acceleration, the transverse and longitudinal rms sizes grow quickly up to about 40 periods due to the instability. With the acceleration, the mismatched rms envelope oscillations growth is significantly damped and the beam becomes stable. Without acceleration, the envelope instability also causes large (more than a factor of 3 and 7) emittance growth. With the acceleration, the emittance growth is small and below 30% through this lattice.

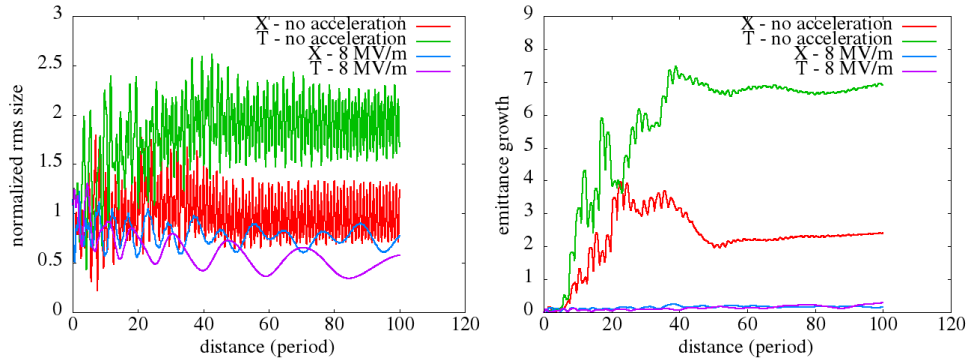


FIG. 3: The horizontal and longitudinal normalized rms size evolution (left) and emittance growth evolution (right) inside the solenoid-RF channel without acceleration and with acceleration. The depressed transverse phase advance is 40 degrees with 120 degree zero current transverse and longitudinal phase advances.

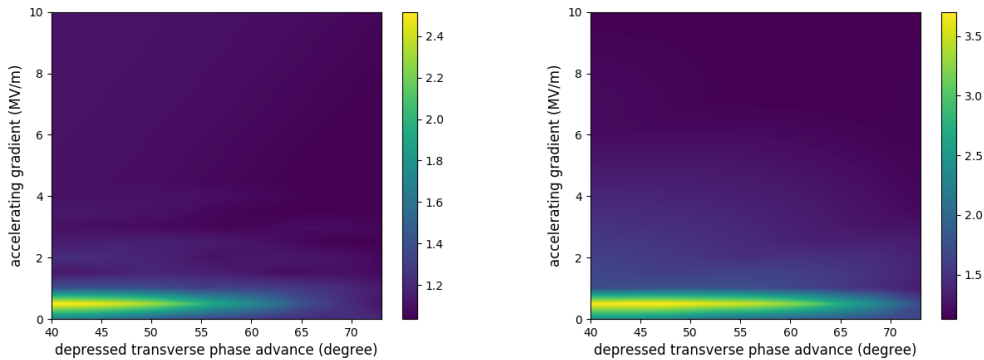


FIG. 4: The maximum normalized horizontal rms amplitude (left) and longitudinal rms amplitude (right) within 100 lattice periods as a function of accelerating gradient and depressed transverse phase advance in the solenoid-RF channel.

To see the effects from acceleration systematically, we calculated the maximum horizontal and longitudinal rms envelope amplitudes (normalized by the corresponding initial matched rms sizes) within 100 lattice periods and the final emittance growth as a function of accelerating gradient and depressed transverse phase advance in Fig. 4 and Fig. 5. Without acceleration or the accelerating gradient is small, the maximum envelope amplitudes are significantly greater than the initial matched rms sizes due to the envelope instability. Most large amplitudes are located around the left corner of the above plot with 40 degree depressed transverse phase advances and small accelerating gradient. This is consistent with the large envelope mode growth rate in the above envelope instability stopband around 40 degree phase advances. With the increase of accelerating gradient, the normalized maximum amplitudes decrease and approach the initial rms sizes. The mitigation of the instability is also seen in the final emittance growth. Most emittance growth occur with accelerating gradient below 1 MV/m due to the instability. With the increase of accelerating gradient, the final emittance growth become smaller and approach a few percent level.

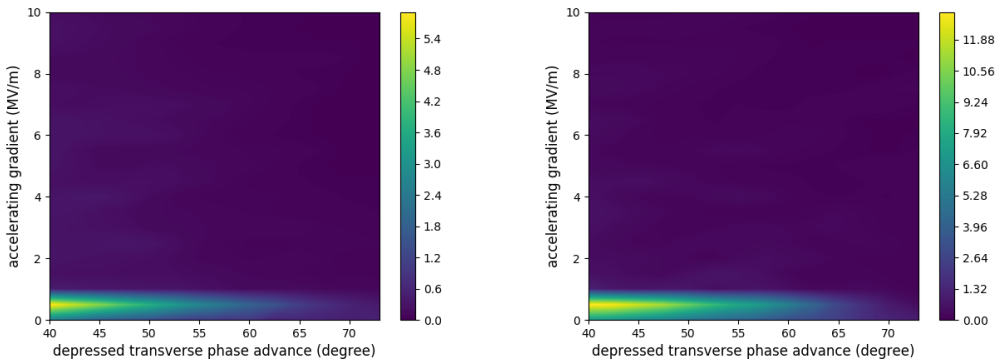


FIG. 5: The final horizontal emittance growth (left) and longitudinal emittance growth (right) at the end of 100 lattice periods as a function of accelerating gradient and depressed transverse phase advance in the solenoid-RF channel.

The acceleration mitigates the envelope instability across the stopbands of depressed phase advance. The acceleration inside the RF cavity provides damping to the envelope oscillation as seen in the envelope equations 3. In addition, both the transverse and the longitudinal focusing strengths depend on the energy of the beam. The space-charge forces also depend on the beam energy. When the beam energy increases due to acceleration, the focusing and the space-charge effects become weaker and helps move the beam out the original instability stopbands.

IV. MITIGATION OF THE ENVELOPE INSTABILITY IN A QUADRUPOLE AND RF CHANNEL

Next, we studied the effects of acceleration on the envelope instability in a transverse quadrupole focusing and longitudinal RF focusing channel using the same proton beam and computational settings. A schematic plot of this

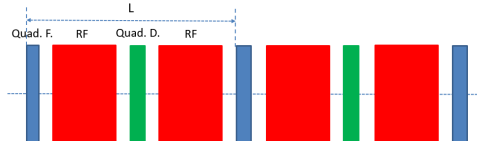


FIG. 6: Schematic plot of a periodic quadrupole and RF channel.

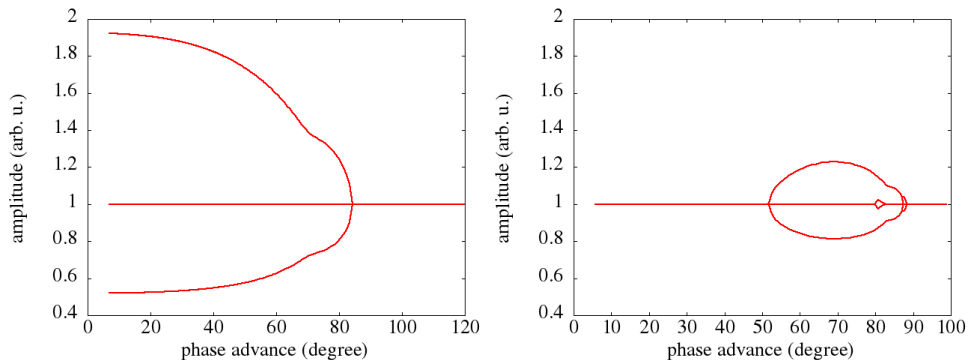


FIG. 7: The 3D envelope mode growth rate amplitudes as a function of depressed transverse phase advance with 120 zero current transverse and longitudinal phase advances in a periodic quadrupole-RF channel without acceleration (left) and with 8 MV/m accelerating gradient (right).

periodic channel is shown in Fig. 6. Each period of the lattice consists of a 0.1 meter focusing quadrupole, a 0.4 meter RF cavity, a 0.1 meter defocusing quadrupole and another 0.4 meter RF cavity. The total length of the period

is 1.4 meters. Figure 7 shows the envelope mode growth rate amplitudes as a function of transverse depressed phase advance inside the above lattice with 120 degree zero current transverse and longitudinal phase advances without and with 8 MV/m accelerating gradient inside the RF cavities. Without acceleration, the beam shows strong envelope instability. Below about 80 degree phase advances, the envelope mode growth rate amplitude is greater than one and becomes larger as the depressed phase advance decreases with stronger space-charge effects. This instability stopband is caused by the confluent resonance of two envelope oscillation modes. With the presence of acceleration, the envelope instability stopband shrinks significantly. Both the stopband width and the growth rate amplitude become much smaller in comparison to those without acceleration.

We also carried out self-consistent macroparticle simulations using the IMPACT code for this lattice. We first selected a point inside the instability stopband with 40 degree depressed transverse phase advances. Figure 8 shows the

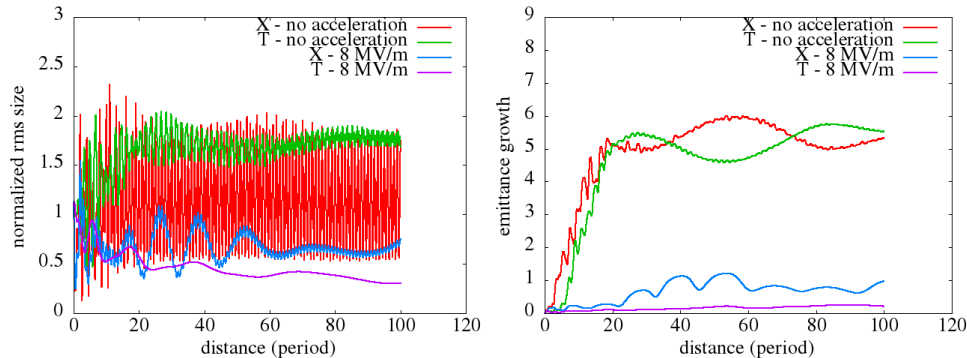


FIG. 8: The horizontal and longitudinal normalized rms size evolution (left) and emittance growth evolution (right) inside the quadrupole-RF channel without acceleration and with acceleration. The depressed transverse phase advance is 40 degrees with 120 degree zero current transverse and longitudinal phase advances.

horizontal and longitudinal normalized rms size evolution and emittance growth evolution through the quadrupole-RF channel without and with 8 MV/m accelerating gradient inside the RF cavities. Without acceleration, both horizontal and longitudinal envelope oscillations are unstable and grow up to about 20 periods before reaching saturation. With the acceleration, except the initial small growth in horizontal plane, the rms sizes decrease and become stable through this lattice. The damping of the longitudinal envelope instability due to acceleration is faster than that of the transverse envelope instability. This could be due to a factor of three larger damping rate in the longitudinal envelope equation in comparison to those in the transverse envelope equations. Without acceleration, the normalized emittances increase by more than a factor of 5 due to the envelope instability. With the acceleration, the longitudinal emittance growth is below 30% and the horizontal growth is below 100%.

Next, we scanned the accelerating gradient inside the RF cavities with depressed transverse phase advance inside the above envelope instability stopband to systematically study the effects of acceleration. Figures 9 and 10 shows

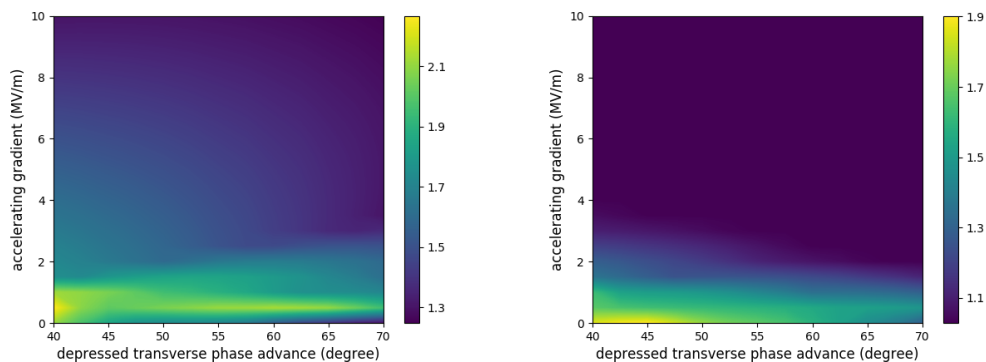


FIG. 9: The maximum normalized horizontal rms amplitude (left) and longitudinal rms amplitude (right) within 100 lattice periods as a function of accelerating gradient and depressed transverse phase advance in the quadrupole-RF channel.

the maximum horizontal and longitudinal rms amplitudes (normalized by the matched rms sizes) within 100 lattice periods and the final emittance growth as a function of accelerating gradient and depressed transverse phase advance.

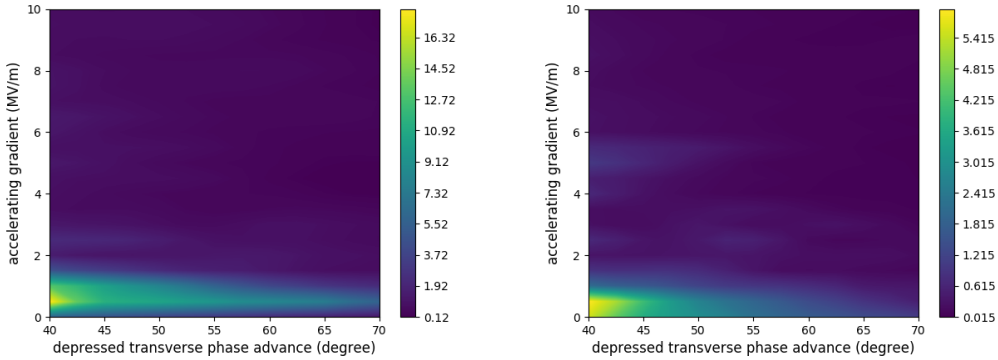


FIG. 10: The final horizontal emittance growth (left) and longitudinal emittance growth (right) at the end of 100 lattice periods as a function of accelerating gradient and depressed transverse phase advance in the quadrupole-RF channel.

With small or zero accelerating gradient, the maximum amplitudes are significantly greater than the matched envelope sizes due to the envelope instability. With the increase of accelerating gradient, the maximum amplitudes become smaller and approach the matched envelope sizes. Most large maximum rms amplitudes are located around the left corner of the plot with small depressed transverse phase advance and accelerating gradient. The mitigation of the envelope instability is also seen in the final emittance growth plot. Most emittance growth occur with an accelerating gradient below 2 MV/m. With the increase of the accelerating gradient, the final horizontal and longitudinal emittance growths become smaller and approach the level of 10%. The acceleration helps mitigate the envelope instability across the stopband of depressed phase advance in this lattice too.

V. CONCLUSIONS

In this paper, we studied the effects of acceleration on the strong envelope instability using a solenoid-RF lattice and a quadrupole-RF lattice with 120 degree zero current phase advances in both transverse and longitudinal directions. We observed that the beam rms envelope oscillation and final emittance growth from the envelope instability were dramatically mitigated due to the RF acceleration in both lattices. This suggests that the restriction of zero current phase advance per lattice period below 90 degrees to avoid the envelope instability in the linear accelerator might be lifted. This opens additional freedom of choosing transverse and longitudinal focusing parameters in the accelerator design that could result in significant cost savings.

ACKNOWLEDGEMENTS

We are grateful for comments by Drs. I. Hofmann and J. Vay and would like to thank Dr. R. D. Ryne for the 3D envelope code. This work was supported by the U.S. Department of Energy under Contract No. DE-AC02-05CH11231 and used computer resources at the National Energy Research Scientific Computing Center.

-
- [1] I. Hofmann, L. J. Laslett, L. Smith, and I. Haber, *Part. Accel.* 13, 145 (1983).
 - [2] J. Struckmeier and M. Reiser, *Part. Accel.* 14, 227 (1984).
 - [3] G. P. Lawrence and T. P. Wangler, in *Proc. of 1997 Particle Accelerator Conference*, p. 1156.
 - [4] J. Stovall, J. H. Billen, S. Nath, H. Takeda, L. M. Young, D. Jeon, K. R. Crandall, R. Shafer, in *Procs. of 2001 Particle Accelerator Conference, Chicago*, p. 446 (2001).
 - [5] Y. Kondo, M. Ikegami, T. Kobayashi, T. Ohkawa, and A. Ueno, *AIP Conference Procs* 773, 79 (2005).
 - [6] F. Gerigk, et al., *Conceptual Design of the SPL II*, CERN-2006-006, 2006.
 - [7] P. N. Ostroumov, *New J. Phys.* 8, 281 (2006).
 - [8] Z. Li et al., *Phys. Rev. ST Accel. Beams* 16, 080101 (2013).
 - [9] M. Eshraqi et al., in *Proc. of the IPAC2014, Dresden, Germany, 2014*, p.3320.
 - [10] M. Aiba, S. Machida, Y. Mori, and S. Ohnuma, *Phys. Rev. ST Accel. Beams* 9, 084001 (2006).

- [11] S.Y. Lee, Phys. Rev. Lett. 97, 104801 (2006).
- [12] S.Y. Lee, G. Franchetti, I. Hofmann, F. Wang, and L. Yang, New J. Phys. 8, 291 (2006).
- [13] G. M. Wang, T. Shaftan, V. Smaluk, Y. Li, and R. Rand, New J. Phys. 8, 291 (2006).
- [14] M. Tiefenback, "Space charge limits on the transport of ion beams in a long alternating gradient system," Ph.D. thesis, Lawrence Berkeley National Laboratory Report LBL-22465, 1986.
- [15] C. Chen and R. C. Davidson, Phys. Rev. Lett. 72, 2195 (1994).
- [16] S. Lee and A. Riabko, Phys. Rev. E 51, 1609 (1995).
- [17] R. Pakter and F. B. Rizzato, Phys. Rev. Lett. 87, 044801 (2001).
- [18] A. V. Fedotov and I. Hofmann, Phys. Rev. Spec. Top.-Accel. Beams 5, 024202 (2002).
- [19] A. V. Fedotov, I. Hofmann, R. L. Gluckstern, and H. Okamoto, Phys. Rev. Spec. Top.-Accel. Beams 6, 094201 (2003).
- [20] S. M. Lund and B. Bukh, Phys. Rev. Spec. Top.-Accel. Beams 7, 024801 (2004).
- [21] L. Groening, W. Barth, W. Bayer, G. Clemente, L. Dahl, P. Forck, P. Gerhard, I. Hofmann, M. S. Kaiser, M. Maier, S. Mickat, and T. Milosic, Phys. Rev. Lett. 102, 234801 (2009).
- [22] D. Jeon, L. Groening, and G. Franchetti, Phys. Rev. Spec. Top.-Accel. Beams 12, 054204 (2009).
- [23] C. Li and Y. L. Zhao, Phys. Rev. ST Accel. Beams 17, 124202 (2014).
- [24] C. Li and Q. Qin, Phys. Plasmas 22, 023108 (2015).
- [25] I. Hofmann and O. Boine-Frankenheim, Phys. Rev. Lett. 115, 204802 (2015).
- [26] D. Jeon, J. H. Jang, and H. Jin, Nucl. Instrum. Methods Phys. Res., A 832, 43 (2016).
- [27] O. Boine-Frankenheim, I. Hofmann, and J. Struckmeier, Phys. Plasmas 23, 090705 (2016).
- [28] I. Hofmann and O. Boine-Frankenheim, Phys. Rev. Accel. Beams 20, 014202 (2017).
- [29] K. Ito, H. Okamoto, Y. Tokashiki, and K. Fukushima, Phys. Rev. Accel. Beams 20, 064201 (2017).
- [30] Y. Yuan, O. Boine-Frankenheim, and I. Hofmann, Phys. Rev. Accel. Beams 20, 104201 (2017).
- [31] I. Hofmann and O. Boine-Frankenheim, Phys. Rev. Lett. 118, 114803, (2017).
- [32] I. Hofmann, "Space Charge Physics for Particle Accelerators," Springer, 2017.
- [33] J. Qiang, Phys. Rev. Accel. Beams 21, 034201 (2018).
- [34] F. J. Sacherer, IEEE Trans. Nucl. Sci. 18, 1101 (1971).
- [35] R. Ryne, Los Alamos Report No. LA-UR-95-391;; <http://xxx.lanl.gov/abs/acc-phys/9502001>.
- [36] T. P. Wangler, RF Linear Accelerators , 2nd ed. (Wiley-VCH, New York, 2008). (Wiley, New York, 2008).
- [37] J. Qiang, R. D. Ryne, S. Habib, and V. Decyk, J. Comput. Phys. 163, 434 (2000).
- [38] J. Qiang, R. D. Ryne, M. Venturini, A. A. Zholents, I. V. Pogorelov, Phys. Rev. ST Accel. Beams, 12, 100702 (2009).